Practical sensorless control for inverter-fed BDCM compressors

H.C. Chen, Y.C. Chang and C.K. Huang

Abstract: Brushless DC motors (BDCMs) possess higher efficiencies than the conventional induction motors and BDCMs have therefore been used widely in inverter-fed compressors. Since the Hall position sensors cannot work well in the high-temperature environment of refrigerants, sensorless control schemes play an important role in the application of inverter-fed BDCM compressors. Sensorless control for actual BDCM compressor is proposed and implemented. First, the sensorless circuits used have been analysed in detail to find the design rules of the circuit parameters for various compressor motors. Then, the limitations of sensorless control are discussed to develop a practical speed controller for BDCM compressors. The developed starting strategy and sensorless algorithms are presented and digitally implemented. Finally, some experimental results are displayed to demonstrate the proposed sensorless speed control for BDCM compressors.

1 Introduction

During the last decades, more and more researchers have focused their attention on energy-saving technology and promoted the development of high-efficiency products. Because that the major power consuming appliances in daily life in many countries are the air conditioning and refrigeration, many manufactures are trying to improve their products' efficiency. Recently, it has been concluded that inverter-fed compressors (or called variable-speed compressors) are the key to increasing system efficiency and reducing energy consumption.

Comparing all the inverter-fed motors such as the induction motors (IMs), synchronous reluctance motors (SRMs) and brushless DC motors (BDCMs) [1, 2], the latter two are free from the excitation loss and rotor copper loss and therefore possess higher efficiencies than the widely used induction motors (IMs) in fixed-speed compressors. Moreover, either because of the unusual power circuits for SRMs or the control complexity of the refrigerant cycle resulting from speed slip of IMs, BDCMs are gradually being applied in the inverter-fed compressors.

To commutate the motor current adequately, the actual rotor positions are required in normal BDCM operation. Unfortunately, in the refrigeration application, high-temperature refrigerants will surround the compressor motor and commonly used rotor-position sensors such as Hall elements cannot be used to sense the positions. To solve this problem, many sensorless control methods have been proposed. They can be divided into two groups according to the motor currents: one is discontinue currents [3–9] (or so-called square-wave currents) and the other is continuous [7] (or so-called sinusoidal-wave currents). Since there always is one motor terminal which is 'floating' in the former group, some schemes, including sensing terminal voltages and diode currents, are used to obtain the rotor positions directly [3–5]. In the latter group, the rotor positions are estimated indirectly through calculation of the *d-q* motor model in MCU/DSP using the feedback motor currents.

In addition, some robust current-control loops are designed in the control structure to improve the performance of sensorless control [6]. The continuous rotor position is obtained from the extended-electromotive-force (EMF) model [7], and thus, it is possible to apply the 180° PWM conduction and SPWM (sinusoidal PWM) methods with continuous current to exploit their reluctance torque. Recently, with the development of IC mixed-signal technology, some sensorless schemes have been implemented into hardware macro cells inside the microcontrollers [8].

In this paper, some simple sensing circuits using passive components are used to obtain the rotor positions from the motor terminal voltages. The analysis and design of the sensing circuits are presented in the following Sections. Furthermore, the simple speed controller will be modified to meet to the limitations of sensorless control and inverter-fed BDCM compressors. All speed-control schemes, including control algorithms and starting strategy, are implemented digitally. Some experimental results are also displayed to demonstrate the proposed sensorless speed control for inverter-fed BDCM compressors.

2 System configuration

The system configuration of the sensorless speed control with BDCM compressor is shown in Fig. 1. After sensing the terminal voltages V_U, V_V, V_W, the sensorless circuits generate the discrete rotor position signals H_U, H_V and H_W. Meanwhile, the starting strategy and sensorless-speed-control algorithms activate in series to drive the BDCM compressor to the desired speed. The BDCM, modelled as Y-connected series with winding impedance Z_X, and electromotive force (EMF) are also drawn in Fig. 1. Both the control strategy and algorithms are implemented digitally in 16-bit MCU (Sun Plus Wel SPMC75F2413A)

© The Institution of Engineering and Technology 2007

doi:10.1049/iet-epa:20060162

Paper first received 27th April and in final revised form 21st July 2006

H.C. Chen is with the Department of Electrical and Control Engineering, National Chiao Tung University, Hsinchu, Taiwan, Republic of China

Y.C. Chang and C.K. Huang are with Energy & Environment Laboratories (EEL), Industrial Technology Research Institute (ITRI), Hsinchu, Taiwan, Republic of China

E-mail: hcchen@mail.nctu.edu.tw

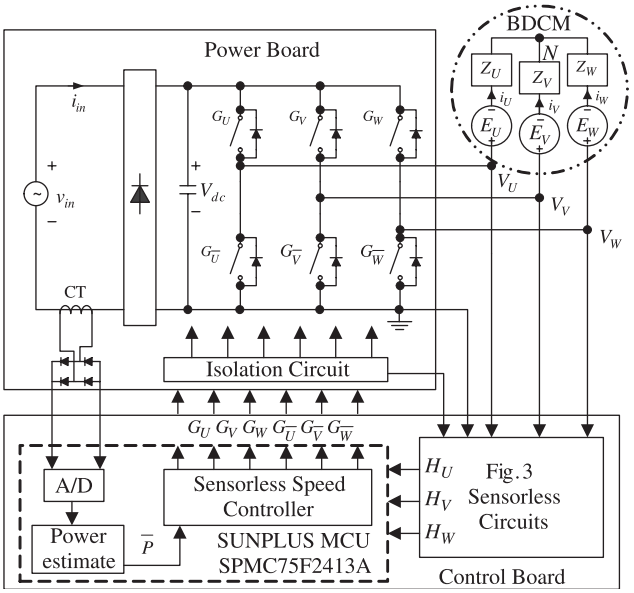

Fig. 1 *System configuration of the sensorless speed control*

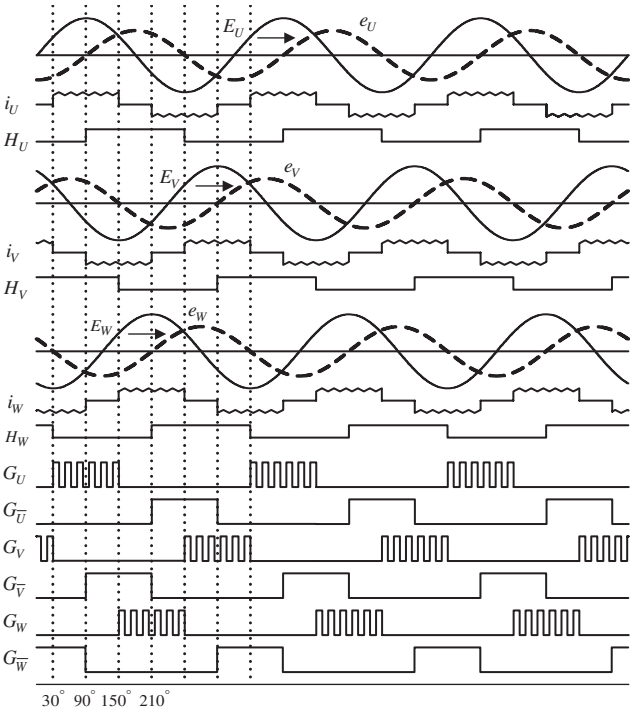

Fig. 2 *Waveforms of the BDCM operation*

which is designed and manufactured to implement the inverter-fed air conditioner.

Figure 2 shows the time charts of the six switching signals G_U–$G_{\overline{W}}$ in normal BDCM operation. To yield adequate motor current by using the well known 120°-PWM-conduction method, the upper three switching signals G_U, G_V and G_W should turn on at 30° lagging the negative-to-positive zero-crossing point of the motor EMFs E_U, E_V and E_W, and turn off at 30° leading the positive-to-negative zero-crossing ones, respectively. Otherwise, the lower three switching signals $G_{\overline{U}}$, $G_{\overline{V}}$ and $G_{\overline{W}}$ should turn on 30° lagging the positive-to-negative zero-crossing point and turn off 30° leading the negative-to-positive zero-crossing ones. However, in the 120°-conduction method, there always is one floating winding, from which we can obtain the EMF and position information without using any position sensors.

3 Sensorless circuits

3.1 Terminal-voltage analysis

As shown in Fig. 1, we can express the terminal voltages V_X as

$$V_X = V_N + E_X + i_X Z_X = V_N + E_X + V_{ZX} X = U, V, W \quad (1)$$

where V_N is the voltage of the motor neutral point, E_X is the respective motor EMF and V_{ZX} presents the voltage drop on the motor-winding impedance Z_X. Since $|V_{ZX}|$ is generally smaller than $|E_X|$ in motor operation, V_{ZX} can be neglected and thus (1) can be rewritten as

$$V_{XN} = V_X - V_N \simeq E_X \quad X = U, V, W \quad (2)$$

Since the duration of each switching pattern is fixed at 60°, the position information hidden in the EMF from (2) can be utilised through generating new signals with either 30°, or 90°, or 150° or 210° phase lagging the terminal voltages V_{XN} within the speed range. Therefore, to keep a constant phase-lagging relation using analogue circuits, the common lowpass-filter circuits are used for their near-constant 90°-phase-lagging characteristics beyond the ten times cut-off frequency.

3.2 Design of sensorless circuits

The sensorless circuit used is shown in Fig. 3 where three identical and independent networks are Y-connected. The transfer function between the terminal voltage V_U and the new signal v_U can be derived as

$$F(s = j2\pi f) = \frac{v_U(s)}{V_U(s)} = \frac{s}{d_3 s^3 + d_2 s^2 + d_1 s + d_0} \quad (3)$$

$$d_3 = R_1 C_1 C_3 R_4 \quad (4)$$

$$d_2 = \left(1 + \frac{R_1}{R_2}\right) C_3 R_4 + (R_1 C_1 + R_1 C_2)\left(1 + \frac{C_3 R_4}{C_2 R_3} + \frac{C_3}{C_2}\right) - R_1 C_2 \quad (5)$$

$$d_1 = \left(1 + \frac{R_1}{R_2}\right)\left(1 + \frac{C_3 R_4}{C_2 R_3} + \frac{C_3}{C_2}\right) + \frac{R_1 C_1 + R_1 C_2}{C_2 R_3} \quad (6)$$

$$d_0 = \left(1 + \frac{R_1}{R_2}\right) \frac{1}{C_2 R_3} \quad (7)$$

where f is the electrical frequency in hertz, P is the pole number and the compressor speed ω_r in revolutions per minute, can be rewritten as $\omega_r = 120 f/P$.

To yield an adequate winding current in the BDCM, the function of the sensorless circuits we have designed is to obtain near-constant 90° phase shifting during the BDCM speed range from the lowest speed ω_{rLow} to the highest

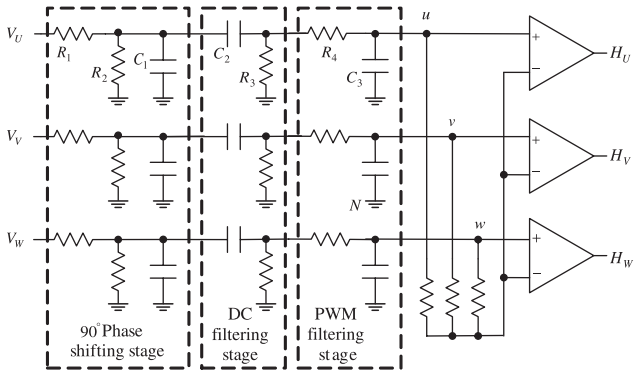

Fig. 3 *Sensorless circuits*

speed ω_{rHigh} in revolution per minute. We can divide the sensorless circuits into three stages: 90°-phase-shifting stage, DC-filtering stage and PWM-filtering stage. The latter two stages are designed to attenuate the undesired low-frequency and high-frequency components in the terminal voltages.

Note that the near-90° phase shifting occurs at a frequency ten times higher than the cut-off frequency of the lowpass filter. Thus, we design a lowpass filter with resistors R_1, R_2 and capacitor C_1 to constitute the first stage. To keep near constant 90°-phase-shifting characteristics, the filter cut-off frequency f_{cut1} must satisfy the rule

$$f_{cut1} = \frac{R_1 + R_2}{2\pi R_1 R_2 C_1} < \frac{1}{10}\left(\frac{P\omega_{rLow}}{120}\right) = \frac{P\omega_{rLow}}{1200} \qquad (8)$$

The DC-filtering stage designed here is to prevent the DC and low-frequency components from appearing in the filtering signals. Therefore, the DC-filtering stage should be a high-pass filter and its cutoff frequency f_{cut2} must be a tenth of the lowest fundamental frequency ($P\omega_{rLow}/120$) so as not to yield extra phase shift within the designed speed range:

$$f_{cut2} = \frac{1}{2\pi R_3 C_2} < \frac{1}{10}\left(\frac{P\omega_{rLow}}{120}\right) = \frac{P\omega_{rLow}}{1200} \qquad (9)$$

Since the PWM frequency f_{PWM} is higher than the speed range, the main function of the last PWM-filtering stage is to attenuate the high-frequency component in signals. Thus, its cut-off frequency f_{cut3} must be placed far smaller than the PWM frequency f_{PWM} and larger than the highest frequency ($P\omega_{rHigh}/120$):

$$\frac{P\omega_{rHigh}}{120} < f_{cut3} = \frac{1}{2\pi R_4 C_3} \ll f_{PWM} \qquad (10)$$

3.3 Design results

In our inverter-fed air conditioner, the PWM switching frequency is $f_{pwm} = 8\,\text{kHz}$ and the 4P BDCM compressor is operating during the speed range between 1000 rev/min ($=\omega_{rLow}$) and 6000 rev/min ($=\omega_{rHigh}$) to yield variable cooling capability. Therefore, it is sensible to select the individual resistor and capacitor values as follows to meet the design rules (8)–(10).

$$R_1 = 470\,\text{k}\Omega, \quad R_2 = 47\,\text{k}\Omega, \quad R_3 = 30\,\text{k}\Omega$$
$$R_4 = 470\,\Omega, \quad C_1 = C_2 = 2.2\,\mu\text{F}, \quad C_3 = 0.47\,\mu\text{F}$$

To ensure the nearly regular 90° phase shift during the speed range, the amplitude and phase responses of the resulting sensorless circuits with different values of resistor R_4 are plotted in Fig. 4.

3.4 Sensorless-commutation table

To obtain the sensorless-commutation table, the assumed 90°-phase-shifting signals e_U, e_V, e_W are also plotted in Fig. 2. In the interval of 30°–90°, the switching signals G_U and $G_{\overline{W}}$ must turn on to yield motor currents i_U and i_W in phase with the motor EMFs E_U and E_W and leave phase V floating, i.e. $i_V = 0$; i.e. when the position signal (H_U, H_V, H_W) are equal to (0, 1, 0), the switching signals G_U and $G_{\overline{W}}$ must be turning on and marked 'PWM' and 'ON' and the other signals turning off and marked 'OFF'. With steps similar to the above, all the conditions can be generated, and they are tabulated in Table 1 where the upper three switches are either 'PWM' or 'OFF' and the lower three switches are either 'ON' or 'OFF'.

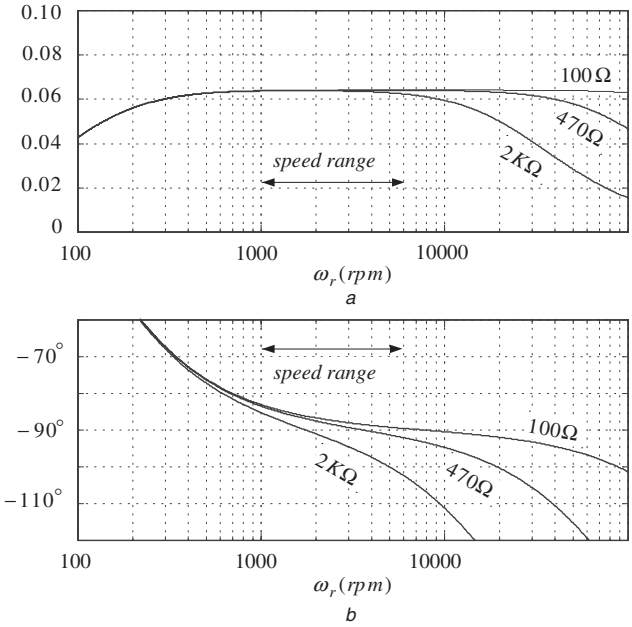

Fig. 4 *Responses of resulting sensorless circuits for different values of resistor R_4*
a Amplitude response
b Phase response

4 Sensorless control

Sensorless control of the BDCM compressor includes the starting strategy and the speed-control loop. The former is very important so that the motor EMFs are zero when the motor is at standstill. Additionally, after considering the limitations of inverter-fed compressors and sensorless control, the final speed-control loop is modified and is far from the conventional speed-control loop.

4.1 Starting strategy

In this study, the proposed starting strategy of the BDCM compressor is divided into three modes: agitation mode, alignment mode and synchronisation mode, as shown in Fig. 5. Before the compressor rotates, the stationary

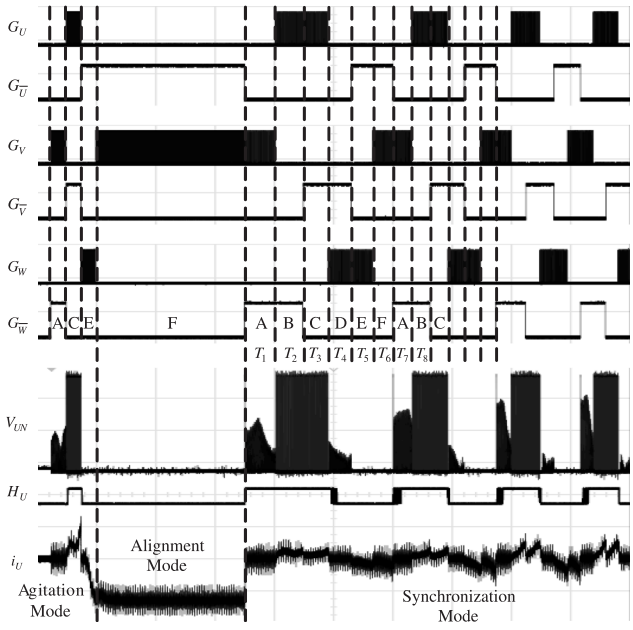

Fig. 5 *Timing diagram of proposed starting strategy*

Table 1: Sensorless-commutation table

(H_U H_V H_W)	G_U	$G_{\bar{W}}$	G_V	$G_{\bar{U}}$	G_W	$G_{\bar{V}}$	Symbol
(0 1 1)	OFF	ON	PWM	OFF	OFF	OFF	A
(0 1 0)	PWM	ON	OFF	OFF	OFF	OFF	B
(1 1 0)	PWM	OFF	OFF	OFF	OFF	ON	C
(1 0 0)	OFF	OFF	OFF	OFF	PWM	ON	D
(1 0 1)	OFF	OFF	OFF	ON	PWM	OFF	E
(0 0 1)	OFF	OFF	PWM	ON	OFF	OFF	F

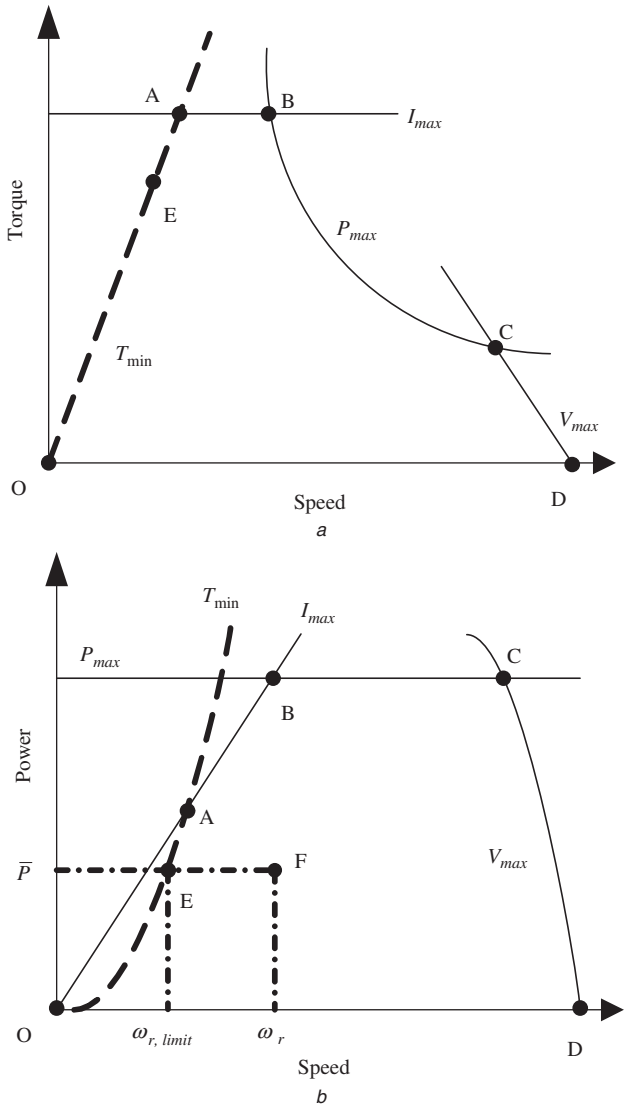

Fig. 6 *Limitations of the sensorless controlled BDCM*
a Torque against speed
b Power against speed

refrigerant is initially agitated to be flowing easily in agitation mode, and then, the rotor is forced to locate in a given position in alignment mode with the commutation state F shown in Table 1. In synchronising mode, the six switching signals G_U–$G_{\bar{W}}$ start changing with the series $A \Rightarrow B \Rightarrow C \Rightarrow D \Rightarrow E \Rightarrow F \Rightarrow A \ldots$ to generate a synchronous rotating magnetic field with increasing rotating speed ω^*_{rsyn}. When the standstill characteristics are known, an optimal acceleration speed rate and the accompanying voltage (PWM duty) can be obtained to lead the rotor

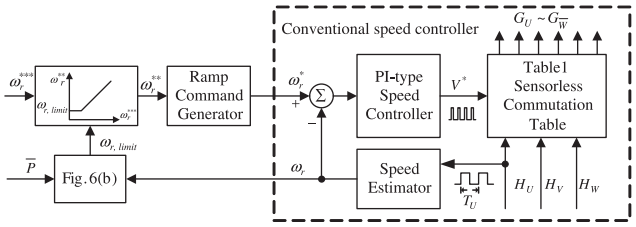

Fig. 7 *Proposed sensorless speed controller for actual BDCM compressors*

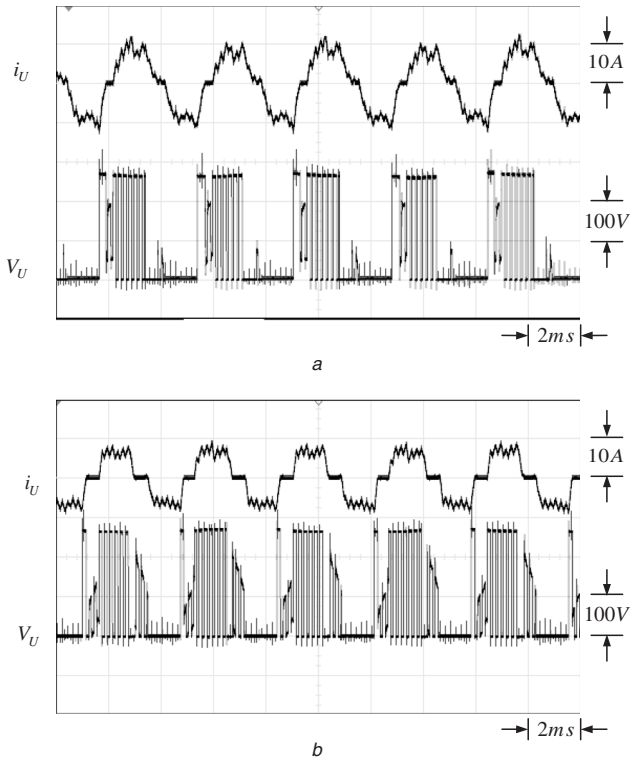

Fig. 8 *Voltage and current waveforms at 5400 rev/min with different values of R_4*
a $R_4 = 2\,\text{k}\Omega$
b $R_4 = 470\,\Omega$

rotating at specified speed synchronously to some speed where the sensorless circuits are able to function well. The period T_n of each commutation state in starting strategy is obtained as

$$T_n = \frac{1}{\left(\frac{P}{2}\right)\left(\frac{\omega^*_{rsyn}}{60}\right)} \times \frac{1}{6} = \frac{20}{P\omega^*_{rsyn}} \tag{11}$$

and the synchronous speed ω^*_{rsyn} can be formulated as

$$\omega^*_{rsyn}(t) = \omega^*_{rsyn0} + \omega^*_{racce} t \tag{12}$$

where ω^*_{racce} denotes the acceleration rate of the compressor for mechanical limitation.

Then, (12) can be rewritten as

$$T_n = \frac{20}{P\left\{\omega^*_{rsyn0} + \omega^*_{racce}\left(\sum_{k=1}^{n-1} T_k\right)\right\}} \tag{13}$$

while the compressor speed ω_r close to the synchronous speed ω^*_{rsyn}, the switching signals G_U–$G_{\bar{W}}$ turn to be determined by the sensorless commutation table in Table 1.

4.2 Limitations

The typical operating characteristics of the BDCM with closed-loop speed control and without flux-weakening operation are shown in Fig. 6*a* where the three solid lines I_{max}, P_{max} and V_{max} are the limitations to mark the BDCM safe-operation region. The line I_{max} is the main limitation at the low-speed region when considering the current-loading ability of the inverter output and the motor windings because the motor EMFs are also low at low speed and the voltage differences on the windings are enough to yield large currents. In the middle-high-speed range, the line P_{max} turns to limit the operating region for the finite inverter-power capability. At high speeds, the motor EMFs are high but the maximum output voltage of the inverter is fixed. Therefore, the V_{max} line follows the P_{max} line to dominate the limitations at high speed because the voltage differences across the motor windings are not enough to yield desired motor current.

In other word, the BDCM operation region is dependent on the traction of the inverter and the motor design. For example, for a motor with relatively low back EMFs (i.e. low K_e), the V_{max} line may disappear and the left-hand two lines I_{max} and P_{max} divide the operation region into the well known constant-torque and constant-power operating regions, respectively. However, note that the sensorless-BDCM-operation region must be further modified.

It is not sensible to neglect the winding-voltage drop V_{ZX} in (1) at low speed and high load torque because V_{ZX} is not significantly smaller than the motor EMF E_X. Therefore, the filtered signals v_{un}, v_{vn}, v_{wn} in Fig. 3 may possess incorrect position signals at low speed and high torque which must result in incorrect current commutation. To avoid unexpected conditions, an extra limiting line T_{min} (dotted line) must be plotted in Fig. 6*a* to limit further the operation region of sensorless controlled BDCM, especially at low speed. Since the motor EMF E_X is increases with

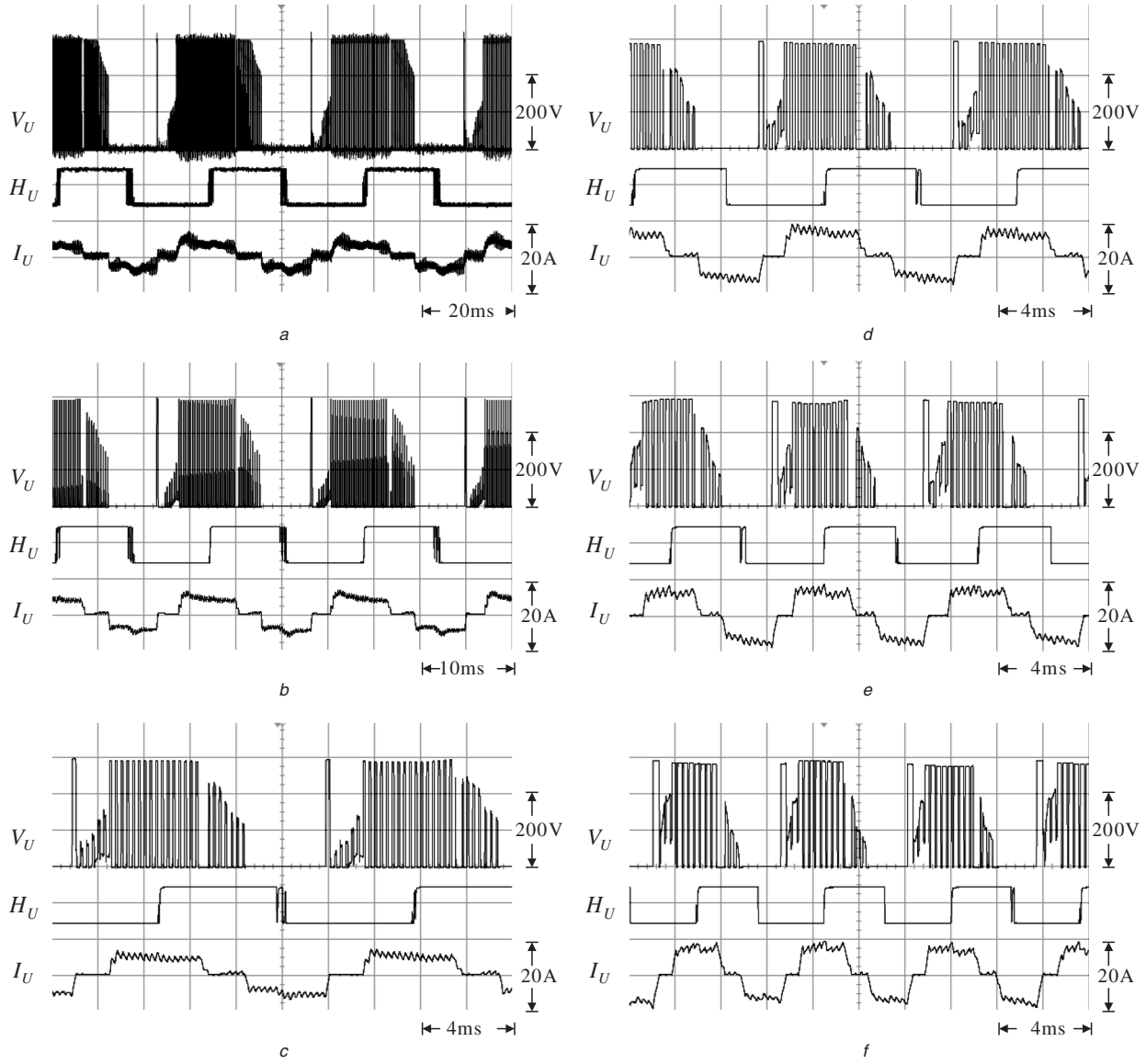

Fig. 9 *Critical waveforms at different speeds*
a 900 rev/min
b 1800 rev/min
c 2700 rev/min
d 3600 rev/min
e 4500 rev/min
f 5400 rev/min

motor speed and voltage drop V_{ZX} is also increasing with torque, the limiting line T_{min} must have a positive slope and initialising from the origin.

4.3 Practical sensorless control

Figure 7 shows the block diagram of the proposed sensorless-control loops including the conventional PI-type speed controller (dashed line) to yield the PWM ratio. The six switching signals G_U–$G_{\overline{W}}$ are chosen according to the feedback position signals H_U, H_V and H_W. The BDCM speed ω_r in revolutions per minute is obtained from the period T_U of signal H_U through counting in the MCU timer:

$$\omega_r = \frac{1}{T_U} \times \frac{60}{\left(\frac{P}{2}\right)} = \frac{120}{PT_U} \tag{14}$$

In practice, the above limiting lines T_{min} will be considered in our sensorless speed controller. After obtaining the front-end input current i_{in} through the current transformer (CT) and the A/D peripherals shown in Fig. 1, we can estimate the input power estimate $\overline{P}$. Then, the estimated power $\overline{P}$ will be co-ordinated in Fig. 6*b* to decide the speed limit $\omega_{r,limit}$ as shown in Fig. 7, i.e., the minimum operation speed $\omega_{r,limit}$ is decided dynamically based on the input-power estimate $\overline{P}$, and the sensorless controlled BDCM will be guaranteed to locate in the safe operation region.

For the mechanical limitations of the inverter-fed compressors, a ramp-command generator is required in the sensorless control loops to limit the accelerating/decelerating rate ω^*_{rate} of compressor speed command. After studying the compressor specifications, the acceleration/deceleration rate of the compressor speed and the initial speed in starting strategy are given $\omega^*_{racce} = 60$ rpm/s and $\omega^*_{rsyn0} = 48$ rev/min, respectively.

5 Experimental results

To demonstrate the performance improvement of the position-sensing circuits we have designed, some terminal voltage and current waveforms at 5400 rev/min with different circuit parameters $R_4 = 2\,\text{k}\Omega$ and $R_4 = 470\,\Omega$ are plotted in Fig. 8.

We find that the current waveform becomes more symmetrical and the current amplitude becomes smaller in Fig. 8*b* than those in Fig. 8*a*. In fact, the real operating-speed range of BDCM compressors had also been extrapolated from 5400 rev/min ($R_4 = 2\,\text{k}\Omega$) to 6600 rev/min ($R_4 = 470\,\Omega$). Additionally, in order to understand the performance at different speeds, the waveforms at 900, 1800, 2700, 3600, 4500 and 5400 rev/min are also shown in Fig. 9.

To investigate the reliability of the sensorless controlled BDCM compressors, the inverter-fed BDCM compressor was set up in a compressor life-test system whose discharge and suction pressures we are automatically controlled by the test system. The proposed sensorless control system then adjusts the compressor BDCM to the desired speed. Some test data are recorded and tabulated in Table 2 until the system balances the pressures at the compressor rated test point where the discharge pressure is 2.65 MPa and the suction pressure is equal to 1.02 MPa. We find that the loading characteristics of the BDCM compressor in the refrigerant-recycling system are much like the constant-torque load for the same motor-current amplitude at different speeds. Inter alia, the cooling capability of inverter-fed compressor is almost proportional to the compressor speed.

Table 2: Experimental data of developed BDCM compressor

Compressor speed, rev/min	3000	3600	4200	4800	5400
Input power, W	803	930	1071	1228	1390
Compressor power, W	752	878	1011	1165	1314
Flowing rate, kg/min	0.97	1.24	1.49	1.74	1.97
Discharge temperature, °C	86.5	85.7	84.5	85.4	85.2
Cooling capability, kcal/hr	2619	3321	4023	4698	5319
Energy-efficiency ratio, kcal/W	3.48	3.78	3.98	4.03	4.05

Discharge/suction pressures: 2.65/1.02 (MPa)
Suction temperature: 35°C

6 Conclusions

This paper develops a sensorless controller for BDCM compressors where the operating limitations of inverter-fed BDCM compressors and sensorless control are considered. To improve the current waveforms, the sensorless circuits are designed and implemented. The control algorithms, including the starting strategy, the sensorless commutation table and the speed-control loops, are all implemented digitally in MCU. Finally, the experimental results also demonstrate the developed controller.

7 Acknowledgment

This work was supported by the Energy R&D foundation funding provided by the Bureau of Energy, Ministry of Economic Affairs in Taiwan, ROC.

8 References

1 Murakami, H., Honda, Y., Kiriyama, H., Morimoto, S., and Takeda, Y.: 'The performance comparison of SPMSM, IPMSM and SynRM in use as air-conditioning compressor'. Proc. IAS'99, 1999, pp. 840–845
2 Soong, W.L., Kliman, G.B., Johnson, R.N., White, R.A., and Miller, J.E.: 'Novel high-speed induction motor for a commercial centrifugal compressor', *IEEE Trans. Ind. Appl.*, 2000, **36**, (3), pp. 706–713
3 Llzuka, K., Uzuhashi, H., Kano, M., Endo, T., and Mohri, K.: 'Microcomputer control for sensorless brushless motor', *IEEE Trans. Ind. Appl.*, 1985, **21**, (4), pp. 595–601
4 Moreira, J.C.: 'Indirect sensing for rotor flux position of permanent magnet AC motors operation in a wide speed range'. Proc. IAS'94, 1994, pp. 401–407
5 Ogasawara, S., and Akagi, H.: 'An approach to position sensorless drive for brushless DC motors', *IEEE Trans. Ind. Appl.*, 1991, **27**, (5), pp. 928–933
6 Chen, H.C., and Liaw, C.M.: 'Current-mode control for sensorless BDCM drive with intelligent commutation tuning', *IEEE Trans. Power Electron.*, 2002, **17**, (5), pp. 747–756
7 Chen, Z., Tomita, M., Doki, S., and Okuma, S.: 'An extended electromotive force model for sensorless control of interior permanent-magnet synchronous motors', *IEEE Trans. Ind. Electron.*, 2003, **50**, (2), pp. 288–295
8 Shao, J., Nolan, D., and Hopkins, T.: 'Improved direct back EMF detection for sensorless brushless DC (BLDC) motor drives'. Proc. APEC'03, 2003, pp. 300–305
9 Chen, H.C., Chang, Y.C., Lin, S.P., Huang, C.M., Chen, Y.C., and Liang, K.Y.: 'Sensorless control for DC inverter-fed compressors'. Proc. APEC'04, 2004, pp. 1106–1110